



ELSEVIER

Contents lists available at ScienceDirect

Data in Brief

journal homepage: www.elsevier.com/locate/dib

Data Article

Values and property charts for anisotropic freeze-cast collagen scaffolds for tissue regeneration



Prajan Divakar, Kaiyang Yin, Ulrike G.K. Wegst*

Thayer School of Engineering, Dartmouth College, Hanover, NH 03755, USA

ARTICLE INFO

Article history:

Received 14 September 2018

Received in revised form

29 October 2018

Accepted 31 October 2018

Available online 3 November 2018

ABSTRACT

Presented in this article are systematic microstructural and mechanical property data for anisotropic collagen scaffolds made by freeze casting. Three applied cooling rates (10 °C/min, 1 °C/min, 0.1 °C/min) and two freezing directions (longitudinal and radial) were used during scaffold manufacture. Utilizing a semi-automated image analysis technique applied to confocal micrographs of fully hydrated scaffolds, pore area, long and short pore axes, and pore aspect ratio were determined. Compression testing was performed to determine scaffold modulus, yield strength, and toughness.

© 2018 The Authors. Published by Elsevier Inc. This is an open access article under the CC BY-NC-ND license (<http://creativecommons.org/licenses/by-nc-nd/4.0/>).

Specifications table

Subject area	<i>Materials science</i>
More specific subject area	<i>Biomaterials</i>
Type of data	<i>Tables and property charts</i>
How data was acquired	<i>Confocal microscopy; Compression testing.</i>
Data format	<i>Analyzed</i>
Experimental factors	<i>Scaffolds soaked in fluorescein for microscopy.</i>
Experimental features	<i>Pore area, long and short pore axes, and pore aspect ratio determined on confocal micrographs. Modulus, yield strength, and toughness (work to 60% strain) for collagen scaffolds.</i>
Data source location	<i>Hanover, NH, United States</i>
Data accessibility	<i>Data in article</i>

DOI of original article: <https://doi.org/10.1016/j.jmbbm.2018.09.012>

* Corresponding author.

E-mail address: Ulrike.Wegst@dartmouth.edu (U.G.K. Wegst).

<https://doi.org/10.1016/j.dib.2018.10.171>

2352-3409/© 2018 The Authors. Published by Elsevier Inc. This is an open access article under the CC BY-NC-ND license (<http://creativecommons.org/licenses/by-nc-nd/4.0/>).

Value of the data

- This systematic data includes quantitative microstructural and mechanical properties for collagen scaffolds made with different applied cooling rates and freezing directions.
- Such data can be compared to those of collagen scaffolds made with similar or different fabrication techniques.
- The data obtained and correlations found for collagen scaffolds invite a comparison with scaffolds made from other biopolymers.

1. Data

Systematic structural and mechanical property data for longitudinally (L) and radially (R) frozen collagen scaffolds at three different applied cooling rates (10 °C/min, 1 °C/min, 0.1 °C/min) from the lower and upper regions (15 mm apart) of the scaffold are reported below. Included are two pore area measurements (one of the void area of the pore, only, the other of the void area of the pore plus half of the cell wall thickness surrounding the void), the lengths of the long and short pore axes, pore aspect ratio, modulus, yield strength, toughness, and overall porosity (Tables 1–6). Property charts illustrating structure-property-processing correlations are provided in Fig. 1.

Table 1

Pore area (mean \pm S.E.) including and excluding the cell wall area for different scaffolds types in the lower scaffold region.

Scaffold type	Applied cooling rate (°C/min)	Pore area with wall (μm^2)	Pore area without wall (μm^2)
Longitudinal	10	812.9 \pm 9.5	638.9 \pm 7.86
	1	1710 \pm 3.0	1388 \pm 22.9
	0.1	5373 \pm 244	4203 \pm 207
Radial	10	7679 \pm 25	6526 \pm 336
	1	17,480 \pm 5	14,550 \pm 669
	0.1	23,630 \pm 280	20,190 \pm 2480

Table 2

Pore aspect ratio, long axis, and short axis (in all cases: mean \pm S.D.) in the lower scaffold region.

Scaffold type	Applied cooling rate (°C/min)	Aspect ratio	Long axis (μm)	Short axis (μm)
Longitudinal	10	1.583 \pm 0.470	39.88 \pm 19.9	25.08 \pm 8.54
	1	1.500 \pm 0.389	55.78 \pm 24.7	37.80 \pm 14.3
	0.1	1.625 \pm 0.463	101.0 \pm 56.7	63.76 \pm 33.0
Radial	10	2.086 \pm 1.05	147.0 \pm 111	69.08 \pm 28.5
	1	2.031 \pm 0.908	213.9 \pm 140	105.3 \pm 42.0
	0.1	1.774 \pm 0.623	205.6 \pm 177	115.7 \pm 75.8

Table 3Modulus, yield strength, and toughness (mean \pm S.E.) in the lower scaffold region.

Scaffold type	Applied cooling rate ($^{\circ}$ C/min)	Modulus (kPa)	Yield strength (kPa)	Toughness (kJ/m ³)
Longitudinal	10	3000 \pm 230	82.5 \pm 2.0	40.0 \pm 3.7
	1	3040 \pm 140	84.7 \pm 5.5	48.8 \pm 2.3
	0.1	2180 \pm 140	93.3 \pm 2.7	59.5 \pm 1.0
Radial	10	779 \pm 220	37.6 \pm 7.1	38.0 \pm 5.7
	1	1280 \pm 110	68.9 \pm 12	51.7 \pm 6.8
	0.1	2290 \pm 700	137 \pm 4.8	75.9 \pm 5.1

Table 4Pore area (mean \pm S.E.) including and excluding the cell wall area for different scaffolds types in the upper scaffold region.

Scaffold type	Applied cooling rate ($^{\circ}$ C/min)	Pore area with wall (μ m ²)	Pore area without wall (μ m ²)
Longitudinal	10	1809 \pm 49	1370 \pm 39.9
	1	3597 \pm 96	2873 \pm 81.4
	0.1	8452 \pm 395	6966 \pm 348
Radial	10	13,810 \pm 1172	11,700 \pm 1060
	1	15,750 \pm 1154	13,110 \pm 981
	0.1	25,670 \pm 3797	22,200 \pm 3520

Table 5Pore aspect ratio, long axis, and short axis (in all cases: mean \pm S.D.) in the upper scaffold region.

Scaffold type	Applied cooling rate ($^{\circ}$ C/min)	Aspect ratio	Long axis (μ m)	Short axis (μ m)
Longitudinal	10	1.730 \pm 0.671	59.43 \pm 41.4	34.58 \pm 17.4
	1	1.564 \pm 0.490	81.14 \pm 43.4	53.01 \pm 22.1
	0.1	1.562 \pm 0.633	123.3 \pm 61.4	83.48 \pm 39.2
Radial	10	2.019 \pm 0.846	187.0 \pm 139	91.52 \pm 49.8
	1	2.310 \pm 1.25	210.0 \pm 168	91.87 \pm 48.3
	0.1	1.927 \pm 0.741	221.3 \pm 203	116.2 \pm 88.8

Table 6Modulus, yield strength, and toughness (mean \pm S.E.) in the upper scaffold region.

Scaffold type	Applied cooling rate ($^{\circ}$ C/min)	Modulus (kPa)	Yield strength (kPa)	Toughness (kJ/m ³)
Longitudinal	10	3770 \pm 240	86.6 \pm 2.7	32.1 \pm 2.0
	1	2050 \pm 220	86.5 \pm 3.2	31.3 \pm 2.2
	0.1	1410 \pm 120	83.0 \pm 2.2	33.1 \pm 3.2
Radial	10	1310 \pm 150	51.3 \pm 3.6	39.3 \pm 0.85
	1	2780 \pm 340	38.8 \pm 7.6	30.4 \pm 3.3
	0.1	3770 \pm 240	86.8 \pm 1.9	48.2 \pm 3.4

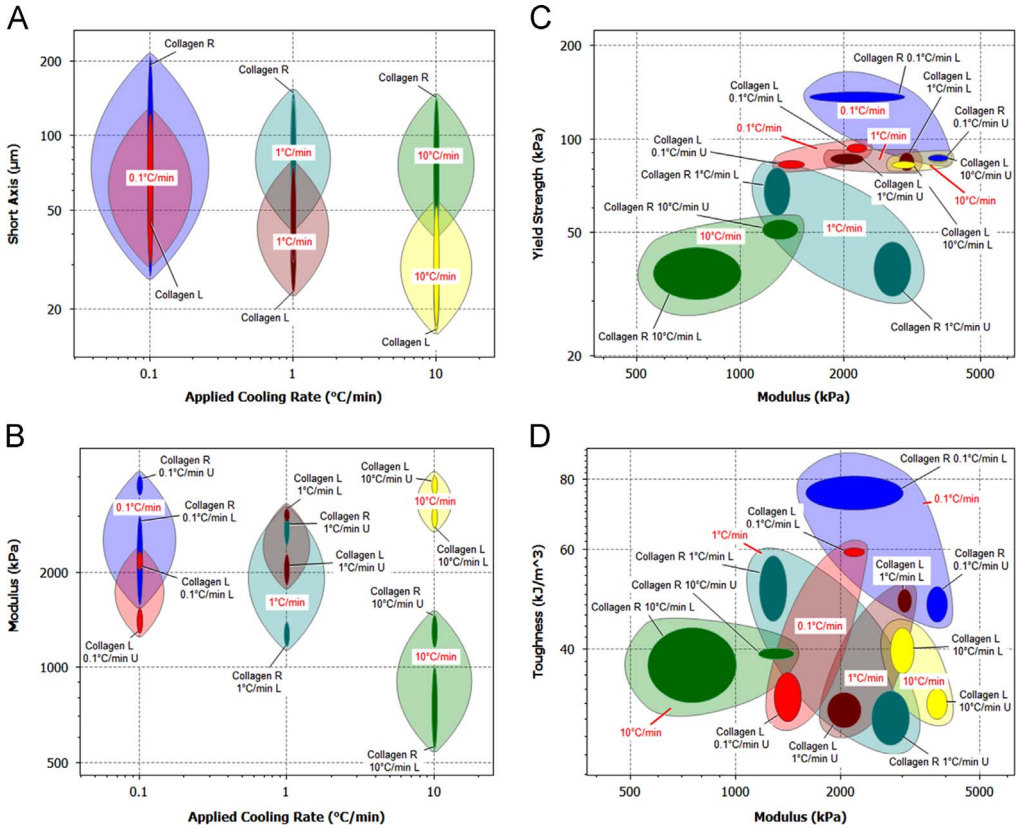


Fig. 1. Property charts illustrating structure-property-processing correlations between (A) pore short axis and applied cooling rate, (B) modulus and applied cooling rate, (C) yield strength and modulus, (D) toughness and modulus for longitudinally (L) and radially (R) frozen collagen scaffolds. Property Charts plotted using the Freeze-Cast Materials Database created with the CES Constructor 2018 Software [1]. The width of the individual material bubbles in the case of the applied cooling rate and length and width of material family bubbles is automatically generated by the CES software. In all other cases the bubble dimensions are defined by the experimental mean plus and minus one standard deviation.

2. Experimental design, materials, and methods

2.1. Slurry preparation

For freeze casting, a 2% (w/v) collagen slurry was prepared by adding 2 g of Type I fibrous bovine tendon collagen powder (Advanced Biomatrix Inc., San Diego, CA) to 0.05 M acetic acid, raising to a total volume of 100 mL, refrigerating the mixture for at least 12 h, and homogenizing (Fisher Scientific™ Homogenizer 152; Fisher Scientific International, Inc., Hampton, NH) thoroughly (at $\sim 3/4$ maximum rpm) for 1.5 h in an ice bath. Prior to freeze casting, slurries (≥ 10 mL) were shear mixed for 3 min at 2200 rpm (Speed Mixer™, DAC 150FVZ-K, FlackTek, Landrum, SC).

2.2. Freeze casting

The collagen slurry was injected with a needle and syringe ($16^{1/2}$ gauge) into 4 mm diameter cylindrical bores of either PTFE molds (25.4 mm diameter; 30 mm length total length; mold bottom: copper) for longitudinal (L) freezing or aluminum molds (25.4 mm diameter; 45 mm total length;

mold bottom: PTFE) for radial (R) freezing [2,3]. Slurries were frozen on copper cold fingers of a standard freeze-casting system [4], at applied cooling rates of 10 °C/min, 1 °C/min, or 0.1 °C/min. Once samples were frozen, the molds were equilibrated to –20 °C in a freezer (HF-5017W-PA, VWR, Radnor, PA) prior to sample punch-out with an Arbor press for lyophilization at 0.008 mBar (–85 °C cooling coil temperature) for at least 24 h in a Freezone 6 Plus system (Labconco, Kansas City, MO).

2.3. Scaffold crosslinking

Freeze-cast and lyophilized collagen-based scaffolds were crosslinked in a solution of 33 mM 1-Ethyl-3-(3-dimethylaminopropyl) carbodiimide (EDC) and 6 mM N-hydroxysuccinimide (NHS) (both Sigma-Aldrich, St. Louis, MO) with 200 proof ethanol as the solvent, and stirred for 6 h at room temperature [5]. Scaffolds were immersed in fresh batches of distilled water and gently stirred for three wash cycles (1 h, 12 h, and 1 h). Before each wash cycle, samples were gently palpated to aid the removal of absorbed solution and residual crosslinking agents. Lastly, samples were soaked in distilled water before flash freezing in liquid nitrogen and lyophilization.

2.4. Confocal microscopy

Scaffolds were imaged in both the lower (7 mm from mold bottom) and upper regions (22 mm from mold bottom) of the scaffold. Transverse scaffold sections (Fig. 1) were prepared using a razor blade (Astra Superior Platinum) and custom-designed 3D printed miter boxes. For imaging, the cylinders were stained in 0.05 mg/mL fluorescein/PBS solution for 24 h on an orbital shaker (VWR International Company, Radnor, PA). Before imaging, samples were gently palpated (at least 3 times) to remove residual fluorescein solution, then immersed in fresh PBS. Imaging was performed with a Nikon A1R Confocal Microscope (Nikon Corporation, Tokyo, Japan) at a 488 nm excitation wavelength and 525/50 nm emission filter; samples were placed on a #1.5 coverslip (0.16–0.19 mm); no Z-stacking was used.

The Imaris (8.4.1) imaging software (Bitplane, Belfast, UK) was used to analyze [6] the transverse confocal micrographs. For longitudinally-frozen scaffolds, analysis was performed on high-magnification micrographs obtained for each sample type; for radially-frozen scaffolds, analysis was performed on micrographs of the entire cross-section obtained for each sample type. Different imaging depths were chosen to accommodate the structural differences between the two freezing directions. The software was used to identify individual pores and measure pore area, lengths of the pore long and short axes, and pore aspect ratio. Two pore area measurements were performed in each case: one of the void area of the pore, only, the other including half of the cell wall thickness surrounding the void (Table 7).

Table 7

Number of pores, n, analyzed per scaffold type and region.

Scaffold type	Applied cooling rate (°C/min)	Lower n	Upper n
Longitudinal	10	4688	1548
	1	2351	1117
	0.1	542	409
Radial	10	683	294
	1	707	344
	0.1	411	172

2.5. Compression testing

Compression tests were performed parallel to the cylinder axis on dry samples of 5 mm length and 4 mm diameter at ambient conditions (22–24 °C and r.h. 52–55%) on an Instron 5498 (Instron, Norwood, MA) with a 50 N load cell at cross-head speed of 0.05 mm s⁻¹ (strain rate of 0.01/s). Compression was chosen to mimic *in vivo* loading conditions [2,3,6–9]. The modulus (the slope of initial linear region), yield strength (yield point, if present, otherwise the intersection of the initial linear slope and the slope of the initially linear plateau region), and toughness (work to 60% strain) were determined from the stress-strain curves. Compression testing was performed on $n = 3$ –5 samples for each of the six scaffold types.

Acknowledgements

The authors thank Ann Lavanway, Matthew Gastinger, and Isabella Caruso for technical and experimental assistance, and both the Thayer School of Engineering and the Department of Biological Sciences, Life Sciences Center, and Dartmouth College Electron Microscopy facilities for their support. This work was supported by National Institutes of Health (NIH-NICHD), USA Award R21HD087828, National Science Foundation (NSF-CMMI), USA Award 1538094, and PD, in part, through a pre-doctoral fellowship awarded under training grant National Institutes of Health (NIH-NIBIB) T32EB021966-01 and the Ph.D. Innovation Program of the Thayer School of Engineering at Dartmouth. The content of this publication is solely the responsibility of the authors and does not necessarily represent the official views of the National Institutes of Health.

Transparency document. Supporting information

Transparency data associated with this article can be found in the online version at <https://doi.org/10.1016/j.dib.2018.10.171>.

References

- [1] CES Constructor & Selector 2018 Software, Granta Design Limited, Rustat House, 62 Clifton Road, Cambridge, CB1 7EG, United Kingdom.
- [2] P. Divakar, I. Caruso, K.L. Moodie, R.N. Theiler, P.J. Hoopes, U.G.K. Wegst, Design, manufacture, and *in vivo* testing of a tissue scaffold for permanent female sterilization by tubal occlusion, *MRS Adv.* 3 (2018) 1685–1690. <https://doi.org/10.1557/adv.2018.57>.
- [3] P. Divakar, B.S. Tremblay, K.L. Moodie, P.J. Hoopes, U.G.K. Wegst, Preliminary assessment of a hysteroscopic fallopian tube heat and biomaterial technology for permanent female sterilization, *Energy-Based Treatment of Tissue and Assessment IX*, International Society for Optics and Photonics (2017) 100660A. <https://doi.org/10.1117/12.2255843>.
- [4] U.G.K. Wegst, M. Schecter, A.E. Donius, P.M. Hunger, *Biomaterials by freeze casting*, *Philos. Trans. R. Soc. A: Math. Phys. Eng. Sci.* 368 (2010) 2099–2121. <https://doi.org/10.1098/rsta.2010.0014>.
- [5] J.S. Pieper, A. Oosterhof, P.J. Dijkstra, J.H. Veerkamp, T.H. van Kuppevelt, Preparation and characterization of porous crosslinked collagenous matrices containing bioavailable chondroitin sulphate, *Biomaterials* 20 (1999) 847–858. [https://doi.org/10.1016/S0142-9612\(98\)00240-3](https://doi.org/10.1016/S0142-9612(98)00240-3).
- [6] P. Divakar, K. Yin, U.G.K. Wegst, Anisotropic freeze-cast collagen scaffolds for tissue regeneration: how processing conditions affect structure and properties in the dry and fully hydrated states, *J. Mech. Behav. Biomed. Mater.* 90 (2019), 350–364. <http://dx.doi.org/10.1016/j.jmbbm.2018.09.012>.
- [7] S. Mohan, I.C. Hernández, W. Wang, K. Yin, C.A. Sundback, U.G.K. Wegst, N. Jowett, Fluorescent reporter mice for nerve guidance conduit assessment: a high-throughput *in vivo* Mode, *Laryngoscope* 128(11), (2018), E386–E392. <http://dx.doi.org/10.1002/lary.27439>.
- [8] K. Yin, P. Divakar, J. Hong, K.L. Moodie, J.M. Rosen, C.A. Sundback, M.K. Matthew, U.G.K. Wegst, Freeze-cast porous chitosan conduit for peripheral nerve repair, *MRS Adv.* 3 (2018) 1677–1683. <https://doi.org/10.1557/adv.2018.194>.
- [9] K. Yin, P. Divakar, U.G.K. Wegst, Freeze casting porous chitosan ureteral stents for improved drainage, *Acta Biomater.* (2018). <http://dx.doi.org/10.1016/j.actbio.2018.11.005>.